ECS Transactions, 80 (10) 171-182 (2017)
10.1149/08010.0171ecst ©The Electrochemical Society

Iron Phosphate Polyanion Compounds as Anodes for Aqueous Lithium-Ion Batteries

Ethan Paharik, Patrick Cantwell, Gary M. Koenig Jr.*
Department of Chemical Engineering, University of Virginia, Charlottesville, VA 22904
*corresponding author: gary.koenig@virginia.edu

Aqueous lithium-ion batteries offer the possibility of the gravimetric capacity, round trip efficiency, and high cycle life of lithium-ion battery materials coupled with the cost and safety advantages of aqueous electrolytes. A common challenge in these systems is the narrow voltage window of aqueous electrolytes and achieving suitable stability of the lithium-ion materials in the electrolyte. This paper will describe synthesis and characterization of iron phosphate compounds as anodes for aqueous lithium-ion batteries. While these materials are at or near the lower range of the stability window of water, oxygen in the electrolyte and subsequent oxygen reduction was the primary challenge in operation of these cells.

1. Introduction

Concern over hydrocarbon price volatility and the negative effects of CO_2 emissions has spurred investments in renewable energy and battery technologies (1). Two of the most prominent renewable energy technologies, wind and solar, generate power intermittently and therefore must be supported by extensive grid level energy storage. Current battery solutions for stationary applications typically rely on aqueous electrolytes, primarily because of their relatively low cost, inflammable solvent, and established operating conditions and maintenance schedules. Many of the existing technologies (such as Ni-MH, Ni-Cd, and Pb-acid) have the drawbacks of relatively low cycle life and round-trip efficiencies less than 75% (2-4), leading to the desire for new active materials for aqueous electrolytes to accommodate the predicted expansion in the stationary energy storage market. Developing a battery that offers high round-trip efficiency, long cycle life, high safety, and high reliability all at a low installed cost would enable electrical energy storage systems at the grid level (3-5).

Recently, a number of research groups have reported using lithium-ion battery active materials with aqueous electrolytes. One key consideration for any battery that uses an aqueous electrolyte is the limited stability window of water (Figure 1). Many commercial cathode materials for lithium-ion batteries such as $LiCoO_2$ (LCO), $LiMn_2O_4$ (LMO) and $LiFePO_4$ (LFP) operate below 4.3 V (vs. Li/Li^+), and thus are near or within the stability window of water. Consequently, lithium-ion cathode materials have been evaluated in aqueous cells including LCO, LFP, and LMO. LMO has been particularly successful as a cathode material in aqueous lithium-ion battery cells. Early aqueous intercalation research by Li and Dahn achieved over 100 mAh/g capacity from LMO cathodes in aqueous electrolyte, although the cells had challenges with regards to cycle life (6). More recent reports for LMO in aqueous electrolyte have included the improvements of attaining capacities of 120 mAh/g and thousands of stable cycles by utilizing techniques such as nano-sizing the particles (7,8) and doping (9,10).

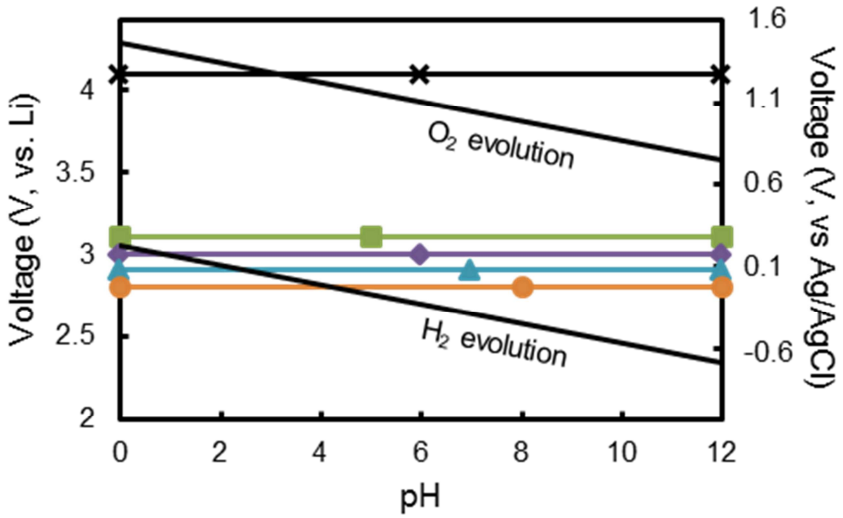

Figure 1. The theoretical electrochemical reaction potentials of the materials used in this study: (A) $LiMn_2O_4$ (✖), (B) $FePO_4$ (■), (C) $Fe_4(P_2O_7)_3$ (♦), (D) $LiFeP_2O_7$ (▲), and (E) $Li_3Fe_2(PO_4)_3$ (●). For reference, the O_2 and H_2 evolution potentials as a function of pH are shown.

Comparatively less progress has been made on aqueous lithium-ion anode materials. Many common commercial lithium-ion anode materials, such as graphite and $Li_4Ti_5O_{12}$, have an intercalation potential that is well over a volt below the stability window of water. Although some battery systems, such as lead acid, have materials that operate outside of the thermodynamic potential window of the aqueous electrolyte, newer battery systems near or outside the water splitting stability window including lithium-ion anode materials have not been well researched. One previously reported aqueous lithium-ion anode material is LiV_3O_8 (11). Another reported aqueous lithium-ion anode materials is $LiTi_2(PO_4)_3$. This material has been paired with LMO to form full cells which have resulted in 82% capacity retention over 200 cycles (12). One of the challenges of using $LiTi_2(PO_4)_3$ is that its potential is still significantly below the water stability window, and thus water splitting and other side reactions have been reported with this material and many reports focus on high rate cycling.

Herein, we will describe electrochemical evaluation of a series of iron polyanion materials as anode candidates for aqueous lithium-ion batteries. The potential for these materials are all very close to the lower stability window of water (Figure 1), suggesting they should be fairly stable for extended cycling. In addition, all of these materials are stably prepared in the delithiated state and thus accept lithium during the first charge and are suitable to pair with existing established aqueous lithium-ion cathode materials such as LMO. Early studies of iron phosphate battery materials were published by Pahdi *et al.* in 1997 with the intent to develop an alternative cathode devoid of expensive and toxic metals (13-14). Of the series of iron phosphate compounds investigated, $LiFePO_4$ (3.5 V vs Li/Li^+) was the most promising cathode material and is now widely researched (15-17). Lower voltage iron phosphate polyanion materials, such as $FePO_4$ (3.2 V vs Li/Li^+), $Fe_4(P_2O_7)_3$ (3.1 V vs Li/Li^+), $LiFeP_2O_7$ (2.9 V vs Li/Li^+), and $Li_3Fe_2(PO_4)_3$ (2.8 V vs Li/Li^+), are less desirable as cathodes but could be suitable for anodes and thus are the focus of this study on using these materials as aqueous lithium-ion anodes. Previous research reports on these iron polyanion materials frequently has focused on addressing low rate capability arising from the intrinsically low electronic conductivity. In all cases,

particle size reduction achieved by ball milling has been successful at dramatically improving electrochemical performance, with up to 50% gains reported in gravimetric capacity (18,19). $FePO_4$ and $Fe_4(P_2O_7)_3$ have also been improved by synthesizing their amorphous hydrates phases, $FePO_4 \cdot 2H_2O$ and $Fe_4(P_2O_7)_3 \cdot 4H_2O$, and not converting the compounds to crystalline or anhydrous phases (19,20). For all four materials, nanoscale size particles are necessary to achieve capacities that approach 120 mAh/g at a rate of C/20. In this work, we will characterize aqueous lithium-ion battery cells comprised of these iron polyanion compounds, and also pair them with LMO to evaluate iron phosphate/LMO aqueous lithium-ion full cells.

2. Experimental

The materials and methods used to synthesize and characterize the iron phosphate battery materials are described below. We note that previous studies of $FePO_4 \cdot 2H_2O$, $LiFeP_2O_7$, and $Li_3Fe_2(PO_4)_3$ were used to guide the synthetic routes used for these compounds (13,21).

2.1 Materials Synthesis

$FePO_4 \cdot 1.9H_2O$ was coprecipitated by adding 24 mL of 0.75 M $NH_4H_2PO_4$ (Sigma-Aldrich) dropwise to a solution of 24 mL 0.75 $Fe(NO_3)_3 \cdot 9H_2O$ (Sigma-Aldrich) and 8 mL 0.25 M citric acid (Fisher). The solution was stirred vigorously for 3 hours at 60 °C. $Fe_4(P_2O_7)_3 \cdot 4.0H_2O$ was synthesized by coprecipitation from $Na_4P_2O_7$ and $Fe(NO_3)_3$. 24 mL of 0.75 M $Na_4P_2O_7$ (Aldrich) was added to 48 ml of 0.375 M $Fe(NO_3)_3 \cdot 9H_2O$ at 50 °C and stirred for 30 minutes. Both powders were vacuum filtered, rinsed with de-ionized (DI) water, and dried in a vacuum oven at 70 °C overnight. The hydrate stoichiometry was determined by thermal gravimetric analysis.

$LiFeP_2O_7$ and $Li_3Fe_2(PO_4)_3$ were synthesized via solid-state reaction between Li_2CO_3 (Fisher), $FeC_2O_4 \cdot 2H_2O$ (Alfa Aesar), and $NH_4H_2PO_4$. These precursors were mixed in the desired stoichiometric amounts and dry milled on a roller with 1 cm diameter zirconia beads for 7 hours. The mixtures were further ground with a mortar and pestle before being heated in air in a box furnace at 300 °C for 2.5 hours to degas the precursors. After regrinding with mortar and pestle, the materials were fired in a tube furnace at 850 °C for 12 and 24 hours for $LiFeP_2O_7$ and $Li_3Fe_2(PO_4)_3$, respectively. The $Li_3Fe_2(PO_4)_3$ sample was again reground by mortar and pestle, and re-fired in the tube furnace at 850 °C for an additional 24 hours.

$LiMn_2O_4$ cathode material was produced via solid-state synthesis between $MnCO_3$ and LiOH (Fisher) at 800 °C for 8 hours in a tube furnace. The $MnCO_3$ precursor was coprecipitated from 0.75 M $MnSO_4 \cdot H_2O$ (Fisher) and 0.75 M Na_2CO_3 (Fisher) in 600 mL DI water (22). The $MnCO_3$ precipitate was vacuum filtered, rinsed with DI water, and dried in a vacuum oven at 70 °C overnight.

2.2 Materials Characterization

The phases of all crystalline materials were confirmed via powder x-ray diffraction (XRD) performed on a diffractometer (PANalytical X'Pert Pro) using a Cu Kα source over a 2θ range of 10-60°. To quantify the structural water content of the materials, TGA was done using a SDT Q600 TG-DTA apparatus (TA Instruments). Samples were dried in a vacuum oven prior to being placed in the TGA where they were

ramped from room temperature to 700 °C at 5 °C /min in flowing 10% O_2 (He balance) atmosphere.

2.3 Electrochemical Methods

The active materials were ball milled with carbon (6.5:1 active to carbon ratio by mass) in a planetary mill (Fritsch) with 3 mm diameter zirconia beads (Fritsch) at 300 RPM for 7.5 hours. Additional carbon was added during electrode prepared from slurries which had the following final composition (by mass): 65% active material, 20% carbon black, and 15% polyvinylidene difluoride (PVDF) binder.

2.3.1 Electrochemical Characterization of Nonaqueous Cells

Thin film electrodes were produced by blending the active material, carbon black, and PVDF binder in a slurry mixer (Thinky) with N-methly-2-pyrrolidone (NMP, Fisher) solvent. The resulting slurry was then spread on a sheet of 20 μm thick aluminum foil and drawn into a film using a doctor blade. The doctor blade height was 150 μm for $LiMn_2O_4$ electrodes and 200 μm for the iron phosphate compound electrodes. The electrode films were dried in an oven at 70 °C overnight and then in a vacuum oven for another 3-4 hours. Electrodes were then punched into 9/16 inch diameter disks. Using these disks, CR2032-type coin cells were constructed in an argon glove box (H_2O < 1 ppm, O_2 < 1 ppm). Polypropylene separators and 1.2 M $LiPF_6$ in 3:7 ethylene carbonate:ethylmethyl carbonate electrolyte were used. Electrochemical tests were performed on a multi-channel battery cycler (MACCOR). Cycling rates were based upon the theoretical capacity of each material, with a rate of 1C corresponding to 145 mA/g for $FePO_4 \cdot 1.9H_2O$, 131 mA/g for $Fe_4(P_2O_7)_3 \cdot 4.0H_2O$, 113 mA/g for $LiFeP_2O_7$, and 128 mA/g for $Li_3Fe_2(PO_4)_3$.

2.3.2 Electrochemical Characterization in Aqueous Electrolyte

Electrodes were also fabricated using the slurries described earlier to coat metal wires rather than aluminum foil. Nickel wires with 1 mm diameters (Goodfellow Cambridge) were cleaned by sonication in 1M HCl (Fisher) and dried. The electrode slurry was then dip-coated onto the nickel wires by hand. The wire electrodes were dried under the same conditions as the thin film electrodes except they were suspended from a support stand in the initial drying step. The various iron phosphate wires had an average loading of 4.0±0.7 mg/cm^2 (corresponding to ~1 mg active material per wire electrode, standard deviation based on over 10 electrodes) and the $LiMn_2O_4$ electrodes an average loading of 3.5±0.7 mg/cm^2 (corresponding to ~0.9 mg active material per wire electrode, standard deviation based on over 10 electrodes). Aqueous electrochemical tests were performed using a three-electrode geometry in a glass cell in 1M Li_2SO_4 electrolyte at pH 9. The pH was adjusted to this value using small amounts of H_2SO_4. A Pt wire was used as the counter electrode and an Ag/AgCl cell as the reference electrode. In full cells, the anode wire was used as both the counter and reference electrode. In all tests, the prepared cell was allowed to sit for at least 30 minutes prior to beginning cycling to ensure wetting of the electrodes and frits. For deoxygenated electrolyte experiments, the test cell was sealed and nitrogen gas was bubbled through the electrolyte during both the 30 minute pre-soak and cycling. Using colorimetric test kits (CHEMetrics), the DO concentration was determined to be between 0.1 and 1 ppm in the deoxygenated electrolyte and between 4 and 5 ppm in the standard electrolyte. Electrochemical experiments were performed using a Reference 600 potentiostat (Gamry).

3. Results and Discussion

3.1 Material characterization

The structures of the synthesized powders were characterized via XRD (data not shown). The crystal phases for LMO, $LiFeP_2O_7$, and $Li_3Fe_2(PO_4)_3$ were consistent with PDF reference patterns 01-078-4144, 01-078-6325, and 04-016-1665, respectively. The LMO material was indexed as having a cubic structure, consistent with previous reports of the Fd3m spinel LMO phase. Refinement of the pattern resulted in a calculated lattice constant of a = 8.254 A. $FePO_4 \cdot 1.9H_2O$ and $Fe_4(P_2O_7)_3 \cdot 4.0H_2O$ did not have peaks in the XRD patterns, and were consistent with amorphous materials. Heating these materials removed the structural water; however, conversion to the crystalline anhydrous phases of these materials had detrimental effects on the electrochemical performance of the materials. Electrochemical tests included in this report were on the amorphous hydrates without any further modification.

3.2 Organic Coin Cell Characterization

The iron phosphate compounds were first evaluated in lithium-ion cells containing organic electrolyte and were used as cathodes paired with lithium metal in half cells and as anodes when paired with LMO in full cells. The charge/discharge profiles of LMO and all phosphate materials in lithium metal half cells at low cycling rates (C/20) can be found in Figure 2. The LMO material demonstrated a reversible capacity exceeding 110 mAh/g (Figure 2A). The phosphate materials are all lithium acceptors and the iron is Fe^{3+}, and thus the cells are all started with discharge cycles accompanied with both lithium insertion and reduction of the iron to Fe^{2+}.

As shown in Figure 2B, the $Li/FePO_4 \cdot 1.9H_2O$ half cell achieved a reversible capacity of 116 mAh/g at an average voltage of 2.92 V, but had an irreversible first cycle capacity loss of 11.4%. The irreversible loss was relatively high, but the total capacity, average voltage, and overall profile shape were consistent with $FePO_4$ materials (20). For $Fe_4(P_2O_7)_3 \cdot 4.0H_2O$, after a first cycle capacity gain of 14.7% there was a reversible capacity of 96 mAh/g at an average voltage of 2.91 V. This capacity corresponded to 2.93 Li^+ ions per unit formula, which was slightly below the previous report of 3 Li^+ per formula unit (13,19).

Average discharge voltages at C/20 (cycle 4) were calculated for all materials (vs. Li/Li^+) and were 2.92 V for $FePO_4 \cdot 1.9H_2O$, 2.91 V for $Fe_4(P_2O_7)_3 \cdot 4.0H_2O$, 2.82 V for $LiFeP_2O_7$, and 2.85 V for $Li_3Fe_2(PO_4)_3$. While these average voltages do not fit the expected trend ($LiFeP_2O_7$ was expected to have a higher voltage than $Li_3Fe_2(PO_4)_3$), the dQ/dV data (data not shown) showed the redox peaks in $Li_3Fe_2(PO_4)_3$ were lower than those of $LiFeP_2O_7$, which was consistent with theory and literature results. These results confirmed the desired electrochemically active materials were synthesized and provided insights into potentials expected for electrochemical activity in aqueous experiments.

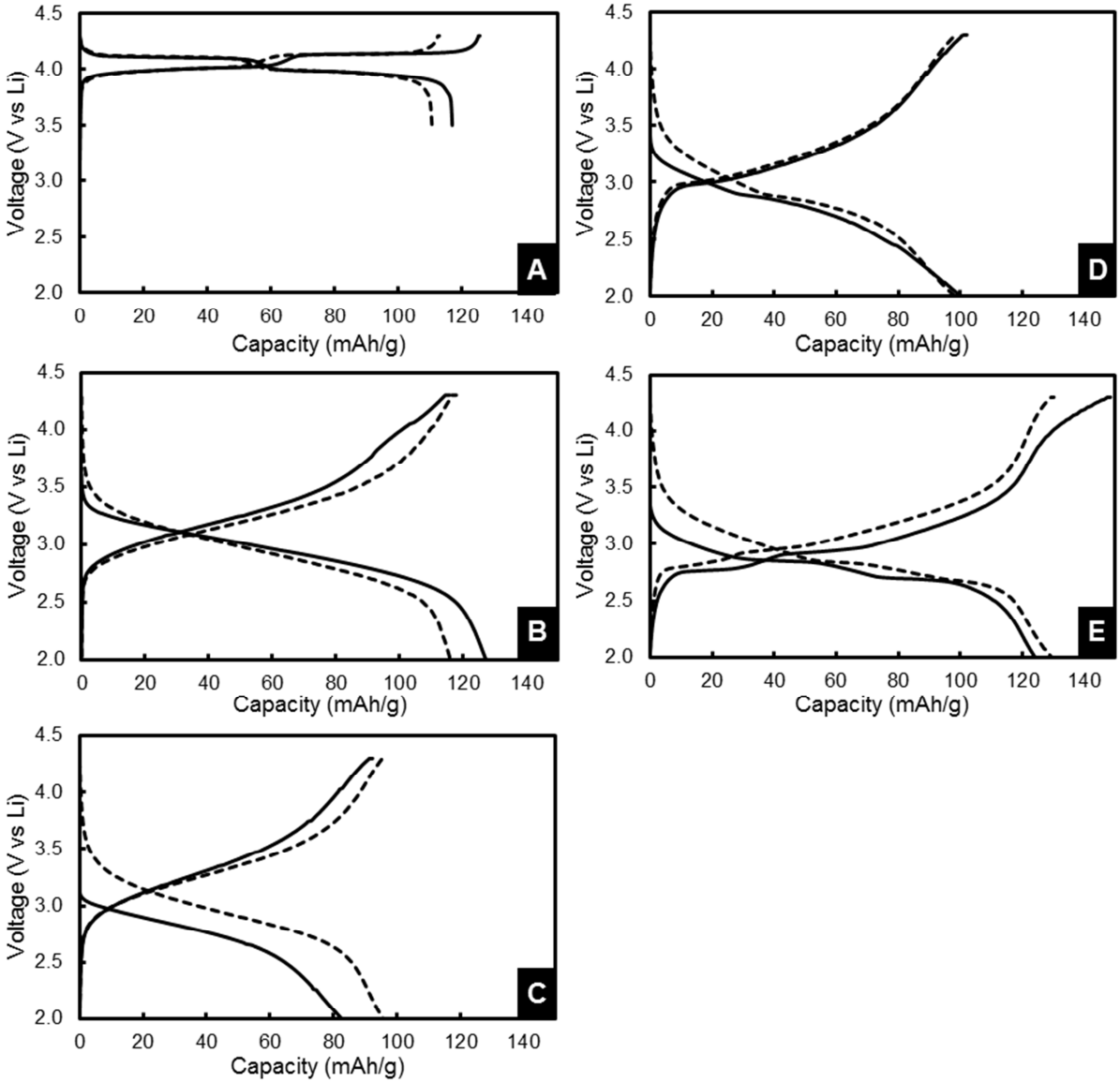

Figure 2. First (–) and fourth (- -) charge/discharge curves of lithium metal half cells paired with electrodes comprised of (A) $LiMn_2O_4$, (B) $FePO_4 \cdot 1.9H_2O$ (C) $Fe_4(P_2O_7)_3 \cdot 4.0H_2O$, (D) $LiFeP_2O_7$, and (E) $Li_3Fe_2(PO_4)_3$. Cells were charged and discharged at a constant rate of C/20 and contained non-aqueous electrolyte.

The experiments in cells containing organic electrolyte demonstrated that the iron phosphate compounds have electrochemical properties consistent with previous reports on these materials. Frequently, these previous studies focused on the suitability of the iron phosphate compounds as potential cathode materials because of their high potential relative to lithium; however, because these materials are lithium accepting we demonstrated full cells in organic electrolytes pairing the iron phosphates as anodes with LMO cathodes (Figure 3). The voltage profiles were consistent with expectations based on half cell cycling of the polyanion anode and LMO cathode materials (Figure 2).

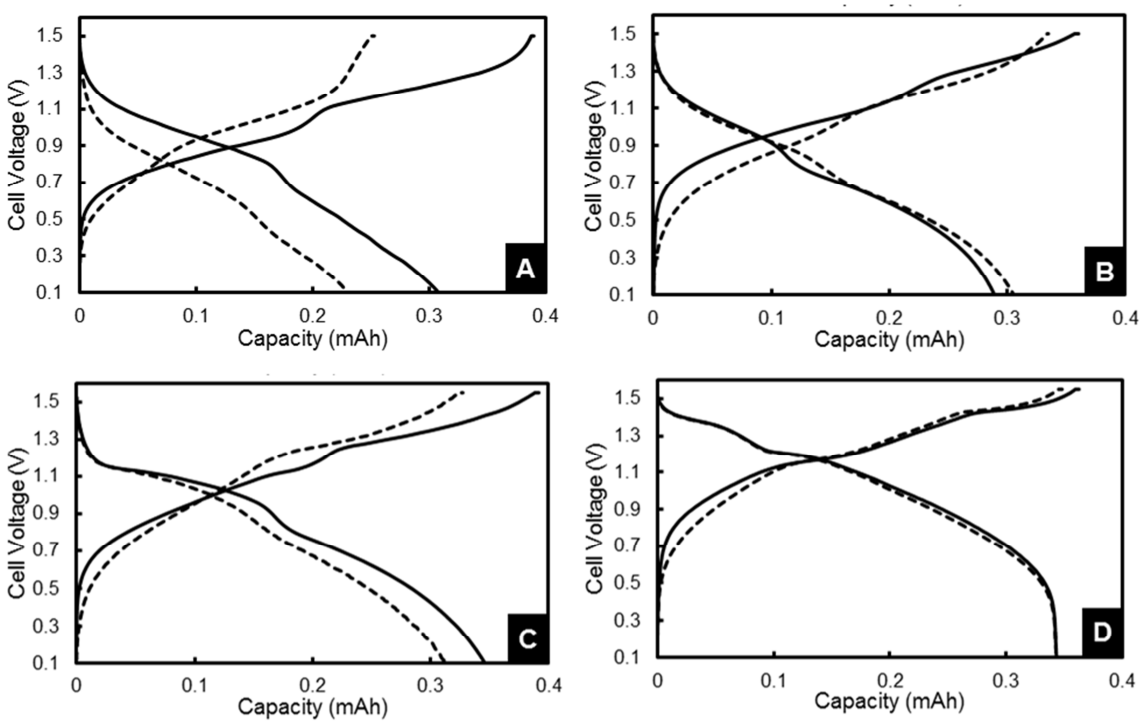

Figure 3. First (–) and fourth (- -) charge/discharge cycles of full cells containing anodes comprised of (A) $FePO_4 \cdot 1.9H_2O$, (B) $Fe_4(P_2O_7)_3 \cdot 4.0H_2O$, (C) $LiFeP_2O_7$, and (D) $Li_3Fe_2(PO_4)_3$ paired with $LiMn_2O_4$ cathodes. Cells were cycled at constant rate of C/20. Active material loading for the anodes and cathodes were (A) 4.23 mg $FePO_4 \cdot 1.9H_2O$ and 3.39 mg $LiMn_2O_4$, (B) 4.36 mg $Fe_4(P_2O_7)_3 \cdot 4.0H_2O$ and 3.30 mg $LiMn_2O_4$, (C) 4.98 mg $LiFeP_2O_7$ and 3.28 mg $LiMn_2O_4$, and (D) 4.16 mg $Li_3Fe_2(PO_4)_3$ and 3.36 mg $LiMn_2O_4$. Cells contain non-aqueous electrolyte.

3.3 Aqueous Electrochemical Characterization

Both the anode and cathode materials were near or within the stability window of water, and thus we prepared aqueous cells (using wire electrodes described in the Experimental section) to explore full cell pairings in aqueous lithium-ion batteries. As shown in Figure 4, the initial charge/discharge profiles at C/2 were very similar to those in the organic electrolyte. While the irreversible first cycle capacity loss and average discharge voltage followed the same trends observed for the organic electrolyte cells, in the aqueous system all the cells had significant capacity fading after even just four discharge cycles. LMO in an aqueous half cell did not have substantial capacity fade (results not shown), and thus the anode with the highest coulombic efficiency, $Li_3Fe_2(PO_4)_3$, was investigated in more detail in aqueous cells.

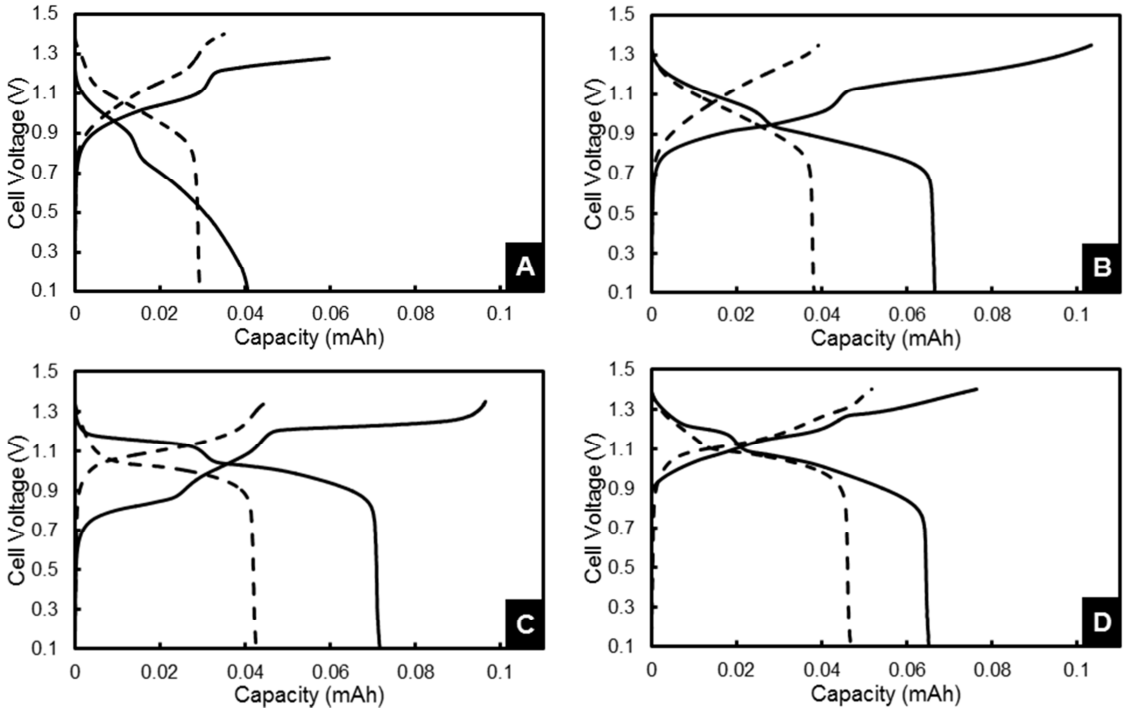

Figure 4. First (–) and fourth (- -) charge/discharge curves of aqueous full cells containing anodes comprised of (A) $FePO_4 \cdot 1.9H_2O$, (B) $Fe_4(P_2O_7)_3 \cdot 4.0H_2O$, (C) $LiFeP_2O_7$, and (D) $Li_3Fe_2(PO_4)_3$ paired with $LiMn_2O_4$ cathodes. Cells were cycled at a constant rate of C/2.

$Li_3Fe_2(PO_4)_3$ electrodes were cycled in aqueous cells (Ag/AgCl reference and Pt counter electrodes) at different rates of charge/discharge both with and without bubbling nitrogen to deoxygenate the electrolyte. The relative capacity on charge compared to discharge for the first cycle at five different rates between C/10 to 2C can be found in Figure 5. In deoxygenated electrolyte, the charge capacity nearly matched the discharge capacity across all rates tested. For the untreated electrolyte that contained an additional ~6 ppm dissolved oxygen, at the highest rate of 2C the charge and discharge capacities were nearly identical, similar to the observations for the deoxygenated electrolyte. However, for the untreated electrolyte the discharge capacity was increasingly greater than the charge capacity at decreasing rates. At the lowest rate of C/10 there was very little charge capacity and the discharge capacity was so great that the test had to be stopped because the cutoff voltage of -0.6 V (vs. Ag/AgCl) was not reached but well above the theoretical capacity of the material had been passed. These results lead us to conclude that at high rates of charge/discharge that the low concentration of dissolved oxygen in the electrolyte results in minimal impact from the oxygen because it was transport limited in arriving to the electrode surface during discharge to oxidize a substantial amount of the $Li_3Fe_2(PO_4)_3$. At slower rates; however, there is sufficient time for the oxygen to reach the $Li_3Fe_2(PO_4)_3$ surface and oxidize the material. This concept is consistent with previous reports for $LiTi_2(PO_4)_3$ materials which can be cycled with high coulombic efficiency in aqueous electrolytes which have not been degassed (12). These cells were typically cycled at high rates of charge/discharge, within the regime where transport of oxygen to the electrode is not fast enough to result in significant capacity from oxygen reduction. Additionally, if these electrodes were cycled in sealed cells the total dissolved oxygen available is much less because the total electrolyte volume is

significantly less (compare ~20 mL of electrolyte in our test system compared to ~0.01 mL of electrolyte in a typical CR2032-type coin cell).

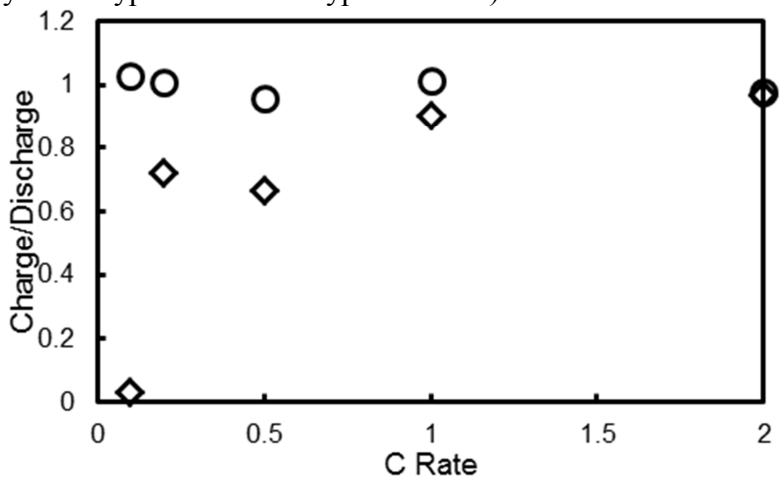

Figure 5. Ratio of charge activity to discharge activity of $Li_3Fe_2(PO_4)_3$ aqueous cells at various rates in (○) deoxygenated electrolyte and (◊) standard electrolyte. Deoxygenation was achieved by bubbling N_2 gas through the electrolyte prior to and during cycling.

After demonstrating the importance of deoxygenating the aqueous electrolyte and with the high observed coulombic efficiency for $LiMn_2O_4$ and $Li_3Fe_2(PO_4)_3$, we performed full cell electrochemical testing with $Li_3Fe_2(PO_4)_3/LiMn_2O_4$ full cells. We tested the cell by performing a rate capability test with charge/discharge rates of C/2, 1C, 2C, 5C, and 10C (3 cycles at each rate, Figure 6A) and followed the rate capability testing with an additional 100 cycles at 1C to show the cycle life of the cell (Figure 6B). After some initial capacity loss in the cell at C/2 due to irreversible capacity loss in the anode and cathode materials, the capacity retention and rate capability were very good. The coulombic efficiency was high and overpotential was low for these electrodes. The round trip energy efficiency for this cell at 1C was >90.

As a final demonstration of the importance of deoxygenating the electrolyte, and $Li_3Fe_2(PO_4)_3$/LMO cell was fabricated and tested using identical materials, processes, and test procedures as done for the results shown in Figure 6, except that the electrolyte was not deoxygenated via nitrogen bubbling. As can be seen in Figure 7, without deoxygenating the electrolyte the coulombic efficiency was always lower than the deoxygenated system, and particularly low during the first 10 cycles. There was also substantial capacity fade in the cell that does not have deoxygenated electrolyte. The problem of dissolved oxygen causing side reactions with the iron phosphate anodes on discharge was consistent with all of the anode materials tested, suggesting that the dissolved oxygen was a significant consideration in aqueous lithium-ion battery anodes. These materials, and others in the literature for aqueous lithium-ion battery chemistry, are well below the oxygen reduction reaction potential and thus there is a strong driving force for this reaction. Previous studies with $LiTi_2(PO_4)_3$ (LTP) have reported that dissolved oxygen in the electrolyte can result in significant irreversible capacity and capacity fade in aqueous lithium-ion cells (12). The irreversible capacity and capacity fade has been attributed to oxidation of the titanium from

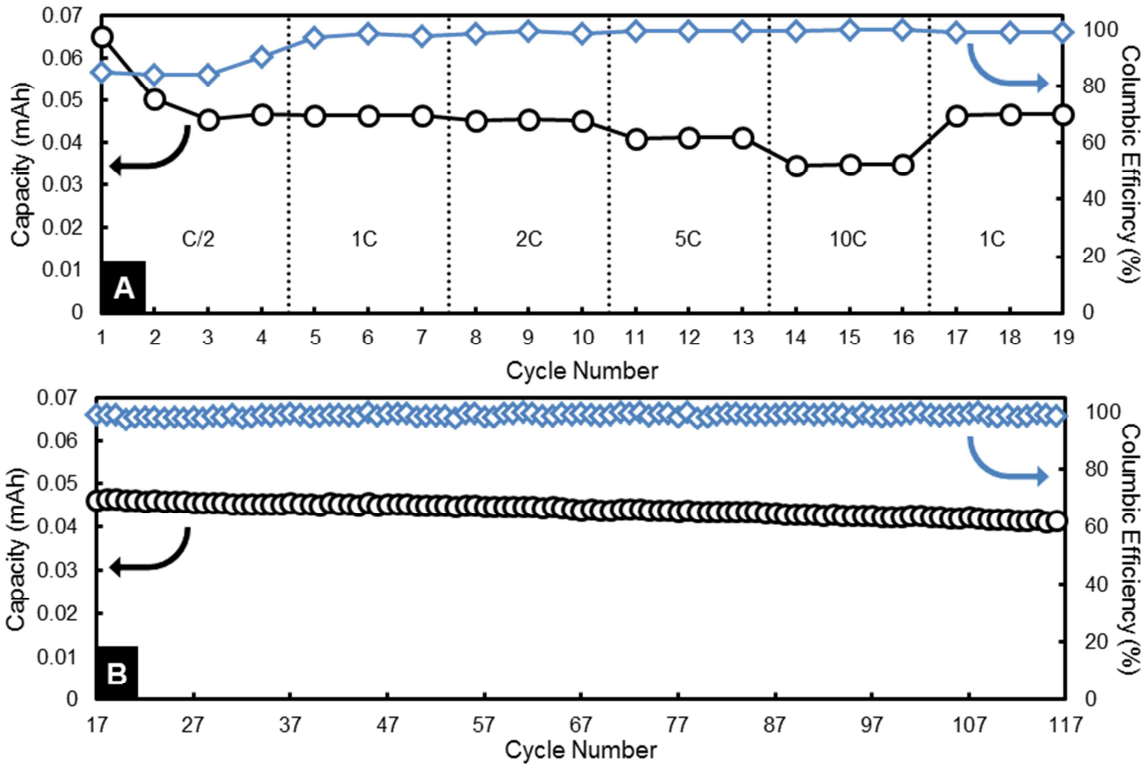

Figure 6. Capacity (left axis,○) and columbic efficiency (right axis,◊) of an aqueous $Li_3Fe_2(PO_4)_3/LiMn_2O_4$ full cell (A) at various rates and (B) for one hundred cycles at a constant rate of 1C. Test was performed in deoxygenated 1M Li_2SO_4. Deoxygenation was achieved by bubbling N_2 gas through the electrolyte prior to and during cycling.

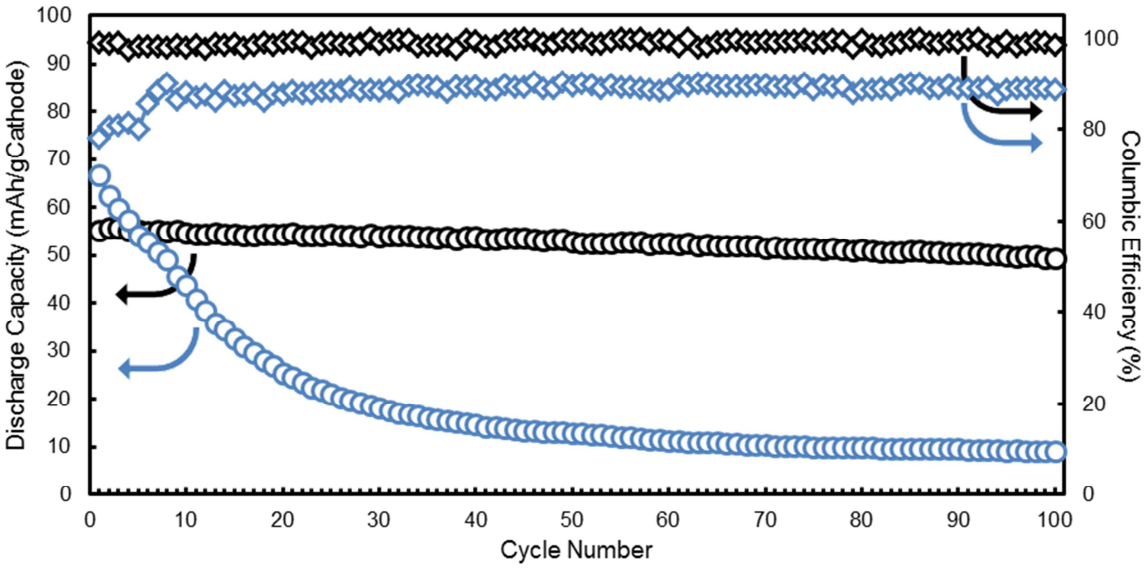

Figure 7. Discharge capacity (left axis,○) and columbic efficiency (right axis,◊) of an aqueous $Li_3Fe_2(PO_4)_3/LiMn_2O_4$ full cell containing deoxygenated electrolyte (black) and standard electrolyte (blue) over 100 cycles at a constant rate of 1C. Deoxygenation was achieved by bubbling N_2 gas through the electrolyte prior to and during cycling.

Ti^{3+} to Ti^{4+} after the titanium was reduced to Ti^{3+} with the corresponding intercalation of lithium into the structure. We speculate that our materials undergo a similar process, with iron being oxidized from Fe^{2+} to Fe^{3+} following the electrochemical reduction of iron to

Fe^{2+} with simultaneous Li^{+} intercalation. On the initial discharge in electrolyte open to the atmosphere and containing ~6 ppm oxygen the iron phosphate anodes have significant irreversible first discharge capacity. In many cases, discharge was stopped because well above the theoretical capacity had been reached and the potential was still above -0.2 V (vs. Ag/AgCl), even though the cutoff discharge potential set for the test was -0.6 V. In contrast, when the electrodes were cycled in an electrolyte in a sealed system that had been bubbled with nitrogen for 30 minutes before cycling to deoxygenate the electrolyte the first cycle capacity irreversible capacity loss was significantly reduced. We note that in sealed cells the dissolved oxygen consumption may not be significant relative to the total cell capacity, but in these experimental cells with relatively large volumes of electrolyte the dissolved oxygen can have a major impact. Cycling at high rates can also overcome some of the effects of having dissolved oxygen within the electrolyte.

4. Conclusion

Four polyanion iron phosphate materials were synthesized and evaluated as lithium-ion electrode materials in both organic and aqueous half cells and full cells. The electrochemical performance, including capacity and rate capability, evaluated in organic electrolyte correlated well with electrochemical evaluation in aqueous electrolyte. Consistent with the potential range of the materials investigated, there was no evidence to suggest significant hydrogen evolution. An oxygen reduction side reaction was a key issue noticed across all materials evaluated. Degassing the electrolyte alleviates this issue but may not be relevant in closed cells with relatively low electrolyte volumes and thus low total oxygen amounts. $Li_3Fe_2(PO_4)_3$/LMO aqueous full cells achieved the best electrochemical performance of the materials investigated, in particular with regards to round trip efficiency and rate capability.

Acknowledgements

This research was in part supported by the National Science Foundation, through award ECCS-1405134.

References

1. B. Dunn, H. Kamath, and J.-M. Tarascon, *Science,* **334,** 928–35 (2011).
2. J. P. Barton and D. G. Infield, *IEEE Trans. Energy Conv.*, **19**, 441-448 (2004).
3. F. Beck and P. Ruetschi, *Electrochim. Acta*, **45**, 2467-2482 (2000).
4. Z. Qi and G. M. Koenig, *J. Vacuum Sci. Tech. B*, **35**, 040801/1-040801/27 (2017).
5. Z. Qi and G. M. Koenig, *J. Power Sources*, **323**, 97-106 (2016).
6. W. Li and J. R. Dahn, *J. Electrochem. Soc.*, **142,** 1742-1746 (1995).
7. G. Yuan, J. Bai, T. N. L. Doan, and P. Chen, *Mater. Lett.,* **137,** 311–314 (2014).
8. Q. Qu, L. Fu, X. Zhan, D. Samuelis, J. Maier, L. Li, S. Tian, Z. Li, Y. Wu, *Energy Environ. Sci.,* **4,** 3985 (2011).
9. J. Yan, J. Wang, H. Liu, Z. Bakenov, D. Gosselink, and P. Chen, *J. Power Sources,* **216,** 222–226 (2012).
10. A. Yuan, L. Tian, W. Xu, and Y. Wang, *J. Power Sources,* **195,** 5032–5038 (2010).
11. J. Kohler, H. Makihara, H. Uegaito, H. Inoue and M. Toki, E*lectrochim. Acta,* **46,** 59-65 (2000).

12. J. Y. Luo and Y. Y. Xia, *Adv. Funct. Mater.,* **17,** 3877–3884 (2007).
13. A. K. Padhi, K. S. Nanjundaswamy, C. Masquelier, S. Okada, and J. B. Goodenough, *J. Electrochem. Soc.*, **144,** 1609–1613 (1997).
14. A. K. Padhi, K. S. Nanjundaswamy, and J. B. Goodenough, *J. Electrochem. Soc.,* **144,** 1188–1193 (1997).
15. M. Takahashi, S. Tobishima, K. Takei, and Y. Sakurai, *Solid State Ionics,* **148,** 283–289 (2002).
16. L. Cheng, G. Liang, S. El Khakani, and D. D. MacNeil, *J. Power Sources,* **242,** 656–661 (2013).
17. G. M. Koenig, J. Ma, B. Key, J. Fink, K.-B. Low, R. Shahbazian-Yassar, and I. Belharouak, *J. Phys. Chem. C*, **117**, 21132-21138 (2013).
18. J. Cabana, J. Shirakawa, M. Nakayama, M. Wakihara, and C. P. Grey, *J. Mater. Chem.,* **21,** 10012 (2011).
19. C. Masquelier, P. Reale, C. Wurm, M. Morcrette, L. Dupont, D. Larcher, *J. Electrochem. Soc.,* **149,** A1037 (2002).
20. C. Delacourt, P. Poizot, D. Bonnin, and C. Masquelier, *J. Electrochem. Soc.,* **156,** A595 (2009).
21. C. Delacourt, C. Wurm, P. Reale, M. Morcrette, and C. Masquelier, *Solid State Ionics,* **173,** 113–118 (2004).
22. J. P. Robinson, G. M. Koenig, *Powder Tech.*, **284**, 225-230 (2015).